Analytical Study of Laterally Loaded Cast-in-Drilled-Hole Piles

SANGCHUL BANG AND C. K. SHEN

This paper summarizes the results of an analytical study of laterally loaded cast-in-drilled-hole (CIDH) piles, which are typically used as the foundations for signposts and sound barrier walls along urban freeways. The CIDH pile derives its bearing capacity from passive earth resistance and is typically considered to be rigid in design and analysis. The analytical formulation, which calculates the ultimate lateral resistance and the point of rotation, considers (a) the nonplane strain soil wedge and (b) the concept of developed friction angle and cohesion to describe the transition of passive lateral earth pressure development from the initial to the ultimate lateral loading condition. Finally, the developed formulation was used to compare the results with those obtained from field and laboratory model testing. Included are comparisons of the ultimate lateral load, the point of rotation, and the distribution of the passive lateral earth pressure.

Cast-in-drilled-hole (CIDH) piles are typically designed as the foundations of posts for large road and commercial signs and for sound barrier walls used to control noise along urban freeways. The CIDH pile derives its bearing capacity from passive earth resistance against translational or rotational lateral movements. It is typically less than 12 ft long with a length-to-diameter ratio ranging from 2 to 1 (for short piles) to about 10 (for longer piles). CIDH piles are considered rigid in their design and analysis because of their low slenderness ratio and high rigidity with respect to the surrounding soil.

This research includes both experimental and analytical investigations with the final objective of establishing an improved design methodology for CIDH piles. The laboratory model testing is intended to (a) provide a thorough understanding of the load transfer mechanism between the soil and the pile, (b) investigate the pertinent parameters that significantly influence the lateral loading capacity and the movement characteristics of the pile, and (c) provide clues for developing an analytical solution method.

A detailed description regarding the laboratory model testing and its results has been already presented (*1*). In this paper the development of the associated analytical solution method is described and the results are compared with the model-testing measurements.

LITERATURE REVIEW

Broms (*2,3*) first attempted to calculate the ultimate lateral resistance of a short rigid pile in cohesive and cohesionless soils. Piles in cohesive soils were assumed to develop a rectangular distribution of lateral soil resistance, starting from a depth of 1.5 times the pile diameter to the tip of the pile with a magnitude of 9 times the undrained shear strength of the soil. Piles in cohesionless soils were assumed to develop a linear lateral soil resistance, which varies from zero at the top to a maximum value at the tip of the pile with a magnitude equal to three times Rankine's passive lateral earth pressure.

Reese et al. (*4*) formulated the ultimate soil resistance of a short rigid pile based on the equilibrium of a tetrahedron-shaped soil failure wedge under lateral load. The total ultimate lateral resistance is calculated from the total passive force minus the active force. The passive force is computed from the geometry of the failure wedge with boundary forces calculated from the Mohr-Coulomb failure criterion, whereas the active force is calculated directly from Rankine's theory. Modifications were later suggested by Matlock (*5*) on the basis of experimental observations.

Ivey (*6*) suggested the inclusion of both the normal and shear stresses developed on all faces of the pile. The distributions of these stresses were assumed to vary along the circumference by cosine and sine functions for normal and shear stresses, respectively. These stresses were summed, and the equilibrium equations of forces and moments were then considered to calculate the ultimate lateral load and the resulting point of pile rotation. The proposed formulation, however, was later modified to satisfy the observed model test results.

Other formulations estimating the ultimate lateral resistance of rigid piles have been proposed by Hays et al. (*7*), Ivey and Dunlap (*8*), Ivey and Hawkins (*9*), Davidson et al. (*10*), Lytton (*11*), Ivey et al. (*12*), Seiler (*13*), Hansen (*14*), as well as others. Generally, the Ivey and Dunlap method and the Ivey and Hawkins method predict conservative values (*15*), whereas the Hansen and Lytton methods yield consistently unconservative values for larger piles (*16*). The Broms method tends to be conservative for stiff clays but unconservative for soft clays (*16*).

Many experimental measurements (*15,17–20*) indicate that (a) the developed passive lateral earth pressure distributions are nonlinear and close to parabolic in shape and (b) the point of rotation is located approximately at 0.7 times the embedded pile length as measured from the ground surface. In most cases, the point of rotation shifts downward from some point below the middle of the embedded pile for lighter loads to a point approximately three-fourths of the embedment depth for maximum lateral load.

Because CIDH piles involve a nonplane strain geometry and a rotational mode of movement, the classical Rankine lateral earth pressure expression may not be directly applicable. In addition, the ultimate lateral load of the CIDH pile

S. Bang, Department of Civil Engineering, South Dakota School of Mines and Technology, Rapid City, S. Dak. 57701. C. K. Shen, Department of Civil Engineering, University of California at Davis, Davis, Calif. 95616.

may not necessarily be obtained at the limiting state (i.e., when the soil develops its full passive resistance along the entire length of the pile).

LABORATORY MODEL TESTING

The testing facility included a large test bin, an instrumented pile, a loading system, and a data-acquisition system. The dimensions of the test bin were 12 ft by 4 ft by 4 ft. The model pile was made of an aluminum tube pipe 0.25 in. thick, 40 in. long, and with an outside diameter of 3.5 in.

The model pile-testing program included the construction of either level or sloping ground embankments made of pit-run air-dried sand or silty clay. Seventeen tests were conducted on sand and 27 tests were on silty clay. Parameters covered in the study were the embedment length of the pile, the type of loading, the direction of loading, the sloping nature of the ground, and the distance of the pile from the slope edge. For each test, parameters such as the load versus displacement response and the lateral earth pressure distributions were measured. A detailed description of the laboratory model testing and its results has been made by Shen et al. (*1*).

THEORETICAL FORMULATION

On the basis of the results obtained from model testing and literature review, it was decided that a reasonable model to analyze the rigid pile-soil interaction behavior should follow the soil failure wedge proposed by Reese et al. (*4*). Furthermore, Dubrova's concept of movement-dependent lateral earth pressure distribution (*21*) was also incorporated and modified to calculate the interface stresses under all intermediate states of lateral loading before failure.

The passive lateral earth pressure developed along the rigid pile can be expressed, in general, as

$$p = p_1 + p_2 + p_3 \tag{1}$$

where

p_1 = lateral earth pressure due to unit weight and soil friction,
p_2 = lateral earth pressure due to cohesion, and
p_3 = lateral earth pressure due to surcharge.

The formulation of passive pressure due to unit weight and soil friction, p_1, can be calculated from the consideration of the soil wedge as shown in Figure 1. One can apply the force equilibrium along vertical and horizontal directions to obtain the developed passive thrust,

$$P = \frac{d}{1 - \tan\delta' \tan\beta}\left(\frac{1}{2}\gamma Z^2 \tan^2\beta + \frac{1}{3}\gamma\frac{Z^3}{d}\tan^3\beta\tan\frac{\phi}{2} - \frac{1}{3}K_0\gamma\frac{Z^3}{d}\tan\beta\tan\frac{\phi}{2} + \frac{2}{3}K_0\gamma\frac{Z^3}{d}\tan\phi\tan\beta\sin\beta\right) \tag{2}$$

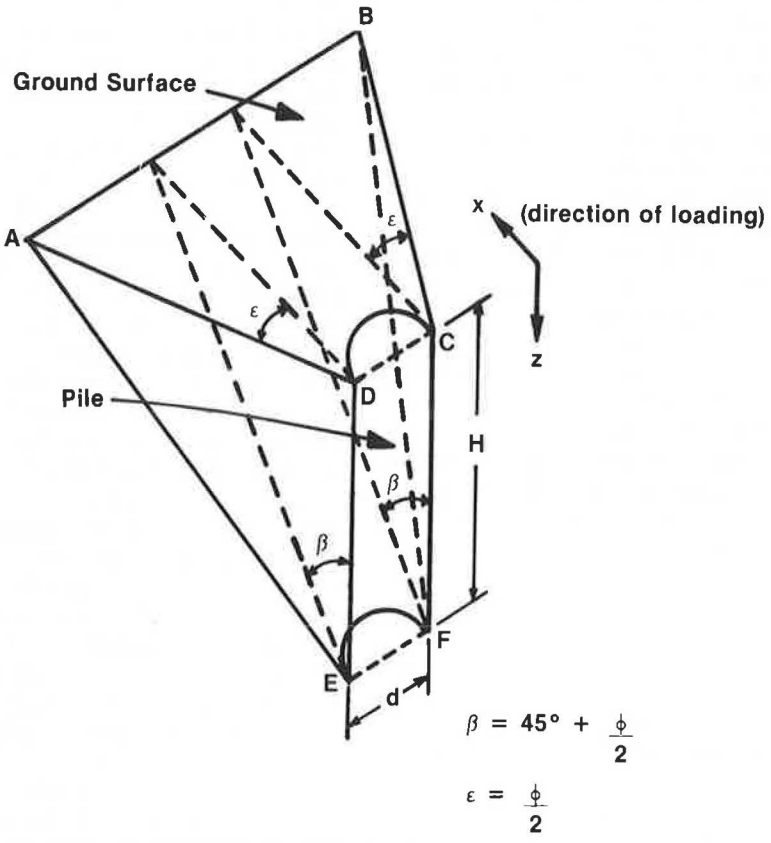

FIGURE 1 Soil wedge under lateral load.

where

δ' = developed friction angle between the pile and the soil,
β = failure wedge inclination angle at the pile tip ($45° + \phi/2$),
d = pile diameter, and
Z = depth from the ground surface to the point of interest.

Note that this expression is obtained at the time of failure (i.e., an inclination angle, $45° + \phi/2$ at the tip of the pile, and an orientation angle, $\phi/2$ at the ground surface, are used). If the inclination and orientation angles have values as described above everywhere along the length of the pile, the ultimate passive lateral earth pressure can be obtained by directly differentiating P with respect to depth Z. However, as discussed in the literature review, it is highly unlikely, particularly in the rotational mode of movement, that the angles reach full values everywhere as described by soil internal friction angle, ϕ. For this reason, it is assumed that the friction angle, ϕ, is replaced by the developed friction angle, $-\psi$, where $\psi = -\phi$ within the depth from the ground surface to where a sufficient lateral movement has taken place to achieve the passive state (i.e., within the failure zone). $\psi = 0$ at the point of no lateral movement (i.e., the point of rotation). Between these two points, a hyperbolic variation is assumed to describe the smooth transition of the values of ψ (Figure 2). For instance, the passive pressure distribution above the rotation point will have the developed friction angle

$$\psi = -1.01\phi + \frac{\phi\,(Z - \xi H)}{2\,\alpha H} + \left\{(0.02\phi)^2 + \left[\frac{\phi\,(Z - \xi H)}{2\,\alpha H}\right]^2\right\}^{1/2} \tag{3}$$

where ξH is the depth from the ground surface to the bottom of the failure zone and αH is the depth to the point of rotation.

In addition, the developed friction angle between the pile and the soil is assumed to be

$$\tan\delta' = -\tan\delta\,\frac{\tan\psi}{\tan\phi} \tag{4}$$

where δ is the maximum wall friction angle available.

Substituting all these parameters and differentiating the thrust, P, with respect to depth, Z, yields the following expression of developed passive lateral earth pressure due to the weight and the friction of the soil.

$$p_1 = -\frac{mA'}{(1 + mA)^2}\left[\frac{1}{2}\gamma Z^2 B - \frac{\gamma Z^3}{3d}(C - K_0 D + 2K_0 E)\right] + \frac{1}{1 + mA}\left[\frac{1}{2}\gamma(2ZB + Z^2 B') - \frac{\gamma}{d}Z^2(C - K_0 D + 2K_0 E) - \frac{1}{3}\frac{\gamma}{d}Z^3(C' - K_0 D' + 2K_0 E')\right] \tag{5}$$

where

$$m = \frac{\tan\delta}{\tan\phi}$$

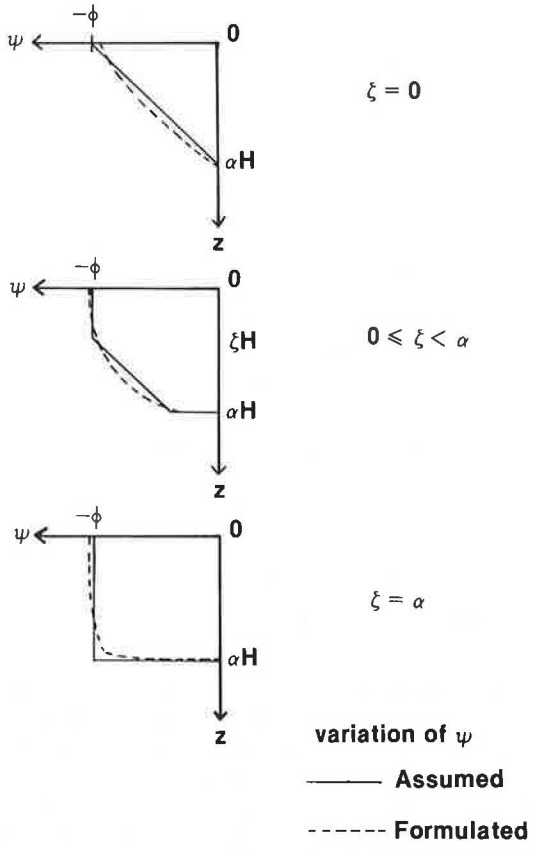

FIGURE 2 Variation of developed friction angle ψ.

$$A = \tan\psi + \tan\left(45° - \frac{\psi}{2}\right)$$

$$B = \tan^2\left(45° - \frac{\psi}{2}\right)$$

$$C = BD$$

$$D = \tan\left(45° - \frac{\psi}{2}\right)\tan\frac{\psi}{2}$$

$$E = A\sin\left(45° - \frac{\psi}{2}\right)$$

$$A' = \frac{\tan\left(45° - \frac{\psi}{2}\right)}{1 + \sin\psi}\frac{d\psi}{dZ}$$

$$B' = \frac{-\tan\left(45° - \frac{\psi}{2}\right)}{\cos^2\left(45° - \frac{\psi}{2}\right)}\frac{d\psi}{dZ}$$

$$C' = B'D + BD'$$

$$D' = \frac{\cos\psi - \sin\psi}{2\cos^2\frac{\psi}{2}(1 + \sin\psi)}\frac{d\psi}{dz}$$

$$E' = A'\sin\left(45° - \frac{\psi}{2}\right) - \frac{1}{2}A\cos\left(45° - \frac{\psi}{2}\right)\frac{d\psi}{dZ}$$

The passive lateral earth pressure distribution due to soil cohesion can be obtained similarly from the wedge considered previously (Figure 1). The resulting expression of the ultimate passive lateral earth pressure becomes

$$p_{2,u} = 3 \tan\left(45° - \frac{\psi}{2}\right) + \frac{\sqrt{2}}{2}\frac{CZ}{d}\tan^2\left(45° - \frac{\psi}{2}\right) \times \left[\cos\left(45° - \frac{\psi}{2}\right) - \tan\frac{\psi}{2}\right] + \frac{\sqrt{2}}{4}\frac{CZ^2}{d}\frac{d\psi}{dZ}\frac{\tan(45° - \psi/2)}{\cos(45° - \psi/2)} \times \left[\frac{\tan\psi/2}{\cos(45° - \psi/2)} - \frac{\sin(45° - \psi/2)}{2\cos^2\psi/2} - \frac{1}{2} - \frac{1}{2}\cos^2(45° - \psi/2)\right] - \frac{3CZ}{2} \times \left[\frac{1}{\cos(45° - \psi/2)}\right]^2\frac{d\psi}{dZ} \quad (6)$$

Note that fully available cohesion is included in this expression. The study should be modified to include the movement-dependent lateral earth pressure development. According to Matlock (*5*), the ratio of the developed versus ultimate pressure of the soft clay depends on the magnitude of movement as shown in Figure 3. Scott (*22*) later approximated this variation using a continuous exponential curve,

$$\frac{p}{p_u} = \left[1 - \exp\left(-\frac{1}{2}\frac{y}{y_c}\right)\right] \quad (7)$$

where y_c equals limiting elastic deformation of the clay.

Consideration of the thickness of the failure zone and the depth to the point of rotation yields an expression of the lateral earth pressure due to cohesion,

$$p_2 = P_{2,u}\left[1 - \exp\left(-4\frac{\alpha - Z/H}{\alpha - \xi}\right)\right] \quad (8)$$

For cases other than those considered (i.e., when stiff clay is considered) and when the point of rotation is located within the upper half of the pile, exactly the same or a virtually identical expression is derived. The detailed derivation is not elaborated, but has been discussed by Shen and Bang (*23*).

The passive pressure development due to ground surcharge, q, can be calculated in a similar manner,

$$p_3 = -\frac{qmA'}{(1 + mA)^2}\left[ZB - \frac{Z^2}{d}(C - K_0D + 2K_0E)\right] + \frac{q}{1 + mA}\left[B + ZB' - 2\frac{Z}{d}(C - K_0D + 2K_0E) - \frac{Z^2}{d}(C' - K_0D' + 2K_0E')\right] \quad (9)$$

where the coefficients were as previously defined for Equation 5.

The combined expression, $p = p_1 + p_2 + p_3$, can now completely describe the transition of the passive lateral earth pressure distribution from an initial failure state (i.e., when the limiting pressure is reached within a single soil element with the largest amount of deformation) to an ultimate failure state. The developed lateral active pressures can be calculated similarly but are neglected because (a) the magnitude of active pressure is virtually insignificant and (b) there may be a separation between the pile and the soil in the active zone, particularly for cohesive soils.

A similar formulation can be developed for the CIDH pile located on or near the sloping ground. Because of the complexity and the number of equations involved, it will not be shown here.

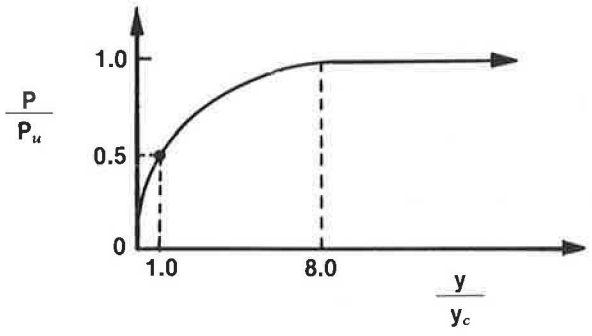

FIGURE 3 Stress-deformation relationship of clay.

ULTIMATE LATERAL LOAD

The distributions of the developed lateral earth pressures need to be modified to incorporate the circumferential variations. Because the normal stress is maximum at $\theta = 0°$ and minimum at $\theta = 90°$, where the angle, θ, is measured from the direction of the loading, one can introduce a cosine function to describe the variation of the normal stress acting on the pile along the circumference as

$$\sigma_r = p' + (p - p')\cos\theta \quad (10)$$

where p is maximum normal stress at $\theta = 0°$ from Equation 1 and p' is minimum normal stress at $\theta = 90°$.

The shear stresses are expressed as

$$\tau^2 = \tau_{r\theta}^2 + \tau_{rz}^2 \quad (11)$$

where $\tau = c + \sigma_r \tan\delta$ and c equals soil cohesion. Note that $\tau_{r\theta} = 0$ at $\theta = 0°$, $\tau_{r\theta}$ = maximum at $\theta = 90°$, τ_{rz} = maximum at $\theta = 0°$, and $\tau_{rz} = 0$ at $\theta = 90°$ (Figure 4). Sine and cosine variations for $\tau_{r\theta}$ and τ_{rz} are therefore assumed.

$$\tau_{r\theta} = (\sigma_r \tan\delta + c)\sin\theta$$

$$\tau_{rz} = (\sigma_r \tan\delta + c)\cos\theta \quad (12)$$

Once the distributions of σ_r, $\tau_{r\theta}$, and τ_{rz} are determined at given depth Z, the corresponding allowable lateral load of a CIDH pile and the corresponding point of rotation can be solved from the equilibrium condition. Figure 4 shows the free-body diagram of a CIDH pile including all the forces acting on it. The developed forces can be obtained from the

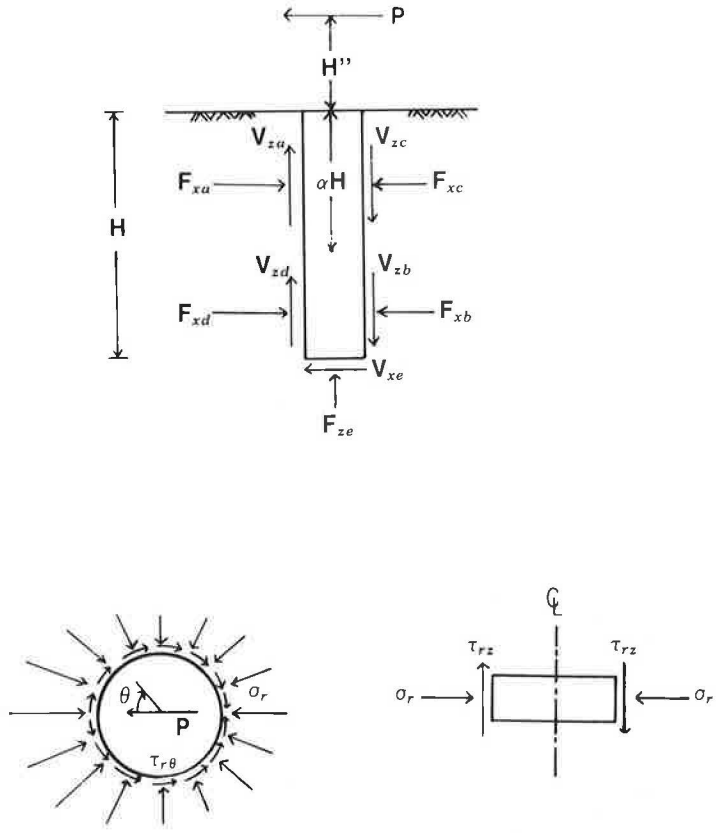

FIGURE 4 Free-body diagram.

integration of stresses acting on the pile. For instance, normal and shear forces acting on the passive side above the rotation point are calculated from

$$F_{xa} = \int_0^{\alpha H} \left[2 \int_0^{\pi/2} \sigma_r \cos\theta \, dA + 2 \int_0^{\pi/2} \tau_{r\theta} \sin\theta \, dA \right] dZ$$

$$V_{za} = \int_0^{\alpha H} \left[2 \int_0^{\pi/2} \tau_{xz} \, dA \right] dZ \qquad (13)$$

Other force components may be obtained in a similar manner.

The detailed analysis of CIDH piles involves an incremental procedure with iterations performed in each increment. Incremental procedure deals with the thickness of the failure zone, ξH, which progresses downward from the ground surface until the ultimate maximum lateral load is obtained. Within each increment, the number of pile segments increases iteratively until convergence is obtained in the solution between two successive values of the number of pile segments.

COMPARISONS

Compared below are the theoretical predictions and the field and laboratory model test results for ultimate lateral resistance and developed lateral earth pressure.

Ultimate Lateral Resistance

Results of 32 model and field tests were compared with the predictions; 20 were from available literature and 12 from the present study. Of the 32 tests, 18 were small-scale models—embedment length of 1 ft or less—and 14 were medium- to large-scale models. The test results covered a variety of soil conditions: 4 in clayey soils, 14 in silty clay soils, and 14 in sandy soils. The present study included 10 tests of CIDH piles in sloping ground.

Table 1 is the summary comparison of the 32 tests. The ultimate lateral resistance (P) and the corresponding point of rotation (α) were computed and compared with the test results. As can be seen, the ratio $P_{\text{measured}}/P_{\text{calculated}}$ (P_m/P_c) varies from 0.63 to 1.78 and the ratio $\alpha_{\text{measured}}/\alpha_{\text{calculated}}$ (α_m/α_c) ranges from 0.78 to 1.28. Note that these comparisons cover a wide variety in geometry of the pile, soil conditions, and ground surface conditions. The comparisons indicate that the proposed method of analysis can predict the ultimate lateral resistance of the CIDH piles reasonably well.

Table 2 shows a comparison of the ultimate lateral resistance values between the test results and those predicted by the several selected methods. On the basis of the information contained in Table 2, the following observations can be made.

1. Hansen's method and Ivey's method give good agreement with the small-scale test results.
2. Davidson's method, on the contrary, agrees reasonably well with the large-scale test results.

TABLE 1 COMPARISON BETWEEN MEASUREMENT AND PREDICTION

Test No.	measured		calculated		Remark
	α	P(lbs)	α	P(lbs)	
Texas C-1	0.56	246	0.57	389	Clay
(12) C-2	0.68	357	0.56	465	
C-3	0.66	290	0.57	348	
L-1	0.73	120	0.57	105	Silt
L-2	0.59	164	0.57	155	
L-3	0.63	238	0.57	217	
Adams (24)	--	25,200	0.64	33,911	
Coyle (16)	--	169,000	0.67	194,010	Pile failure
Texas E-1	0.46	498	0.57	337	Silt
(12) E-2	0.53	410	0.55	255	
E-3	0.54	500	0.56	407	
E-4	0.64	615	0.60	663	
E-5	0.63	352	0.57	309	
Davis Sand	0.67	1,000	0.74	1,092	
Texas S-1	0.65	27	0.73	20	Sand
(12) S-5	0.63	20	0.74	12	
S-12	0.60	34	0.74	20	
S-13	0.67	22	0.72	17	
S-14	0.58	48	0.74	27	
S-16	0.63	52	0.74	31	
S-17	0.69	115	0.78	73	
Davis 7	--	2,650	0.63	3,346	
10	0.72	1,900	0.70	2,196	Downslope loading
13	--	1,480	0.70	2,125	Downslope loading
Davis 19	0.74	1,050	0.70	1,666	Downslope loading
22	0.72	1,822	0.69	2,598	Downslope loading
Davis S-7	0.79	450	0.69	581	Downslope loading
S-9	0.84	520	0.69	586	Downslope loading
S-11	--	540	0.69	582	Downslope loading
S-12	0.73	880	0.73	980	Upslope loading
S-13	0.80	900	0.73	986	Upslope loading
S-14	0.86	875	0.73	981	Upslope loading

TABLE 2 COMPARISON OF ULTIMATE LATERAL LOADS BY VARIOUS METHODS

Test	Ultimate Lateral Load (lbs)				
	measured	Ivey method	Davidson method	Hansen method	Current study
Texas S-1	27	32.5	15.8		20
(12) S-5	20	23.9	11		12
S-12	34	38.2	17.2		20
S-13	22	23.3	11.9		17
S-14	48	50.8	18.6		27
S-16	52	52.5	24.7		31
S-17	115	134	57.3		73
E-1	498	459	241.8	459	337
E-2	410	337	179	388	255
E-3	500	535	249.7	582	407
E-4	615	871	414.4	975	663
E-5	352	384	204.9	481	309
C-1	246	300	271.1		389
C-2	357	344	333		465
C-3	290	241	274.5		348
L-1	120	92			105
L-2	164	154			155
L-3	238	324			217
Davis 7	2,650	8,446	1,871	9,665	3,346
Adams (24)	25,200	52,165	29,558	51,780	33,911
Coyle (16)	169,000	103,301	195,133	242,332	194,010

3. The proposed method of analysis seems to produce the closest predictions of ultimate lateral resistance.

Lateral Earth Pressure

The following are the comparisons of the predicted and measured lateral earth pressure along the length of CIDH piles in both level and sloping embankments. Note that all the lateral earth pressure values are those acting along the direction of the lateral load application ($\theta = 0°$).

Level Sandy Embankment

Five tests with the same soil properties and pile geometry were performed. Figures 5 and 6 show the lateral earth pressure comparisons on the passive sides at horizontal loads of approximately 200 and 1,000 lb, respectively. The measured pressures are expressed by two lines (i.e., upper and lower bounds of five measurements). These comparisons indicate that the proposed method of analysis can predict not only the magnitude of lateral earth pressure but also the approximate distribution. In general, the predicted values lie within the range of measured values.

Sloping Sandy Embankment

The test results of a model CIDH pile installed in a sloping sandy embankment with the lateral load applied away from the slope were compared. Comparison is made at the lateral load of approximately 250 lb as shown in Figure 7. As indicated, the prediction by the proposed method of analysis yields fairly good agreement with the model measurements, both in magnitude and in distribution.

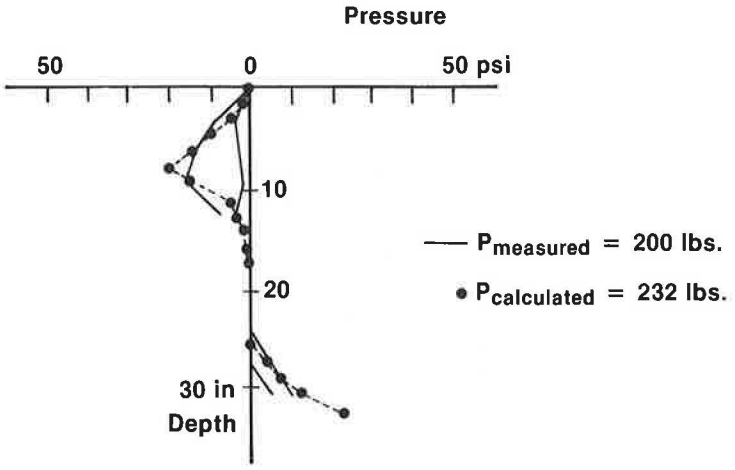

FIGURE 5 Lateral earth pressure comparison—level sand 1 (Test no. Davis sand).

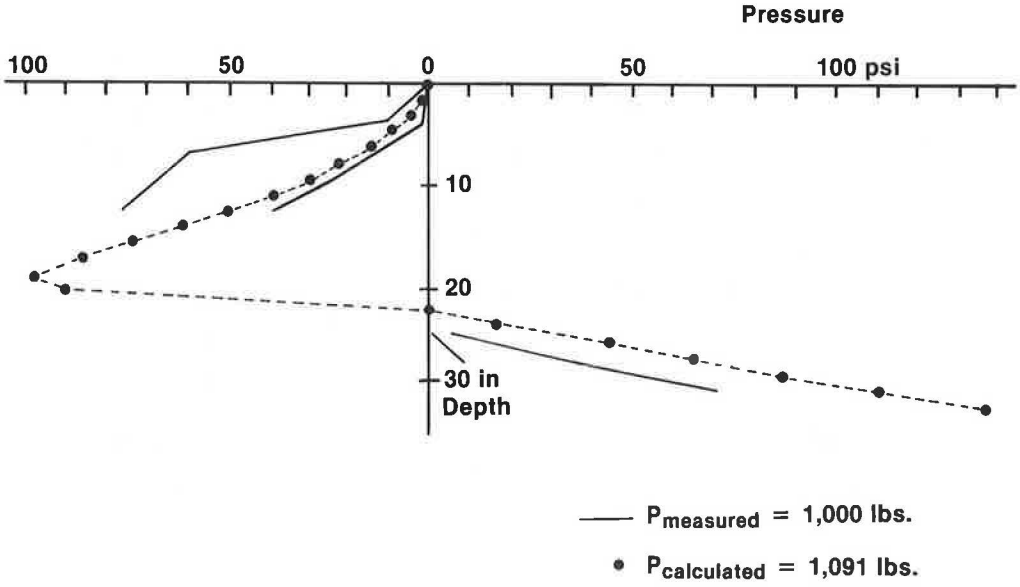

FIGURE 6 Lateral earth pressure comparison—level sand 2 (Test no. Davis sand).

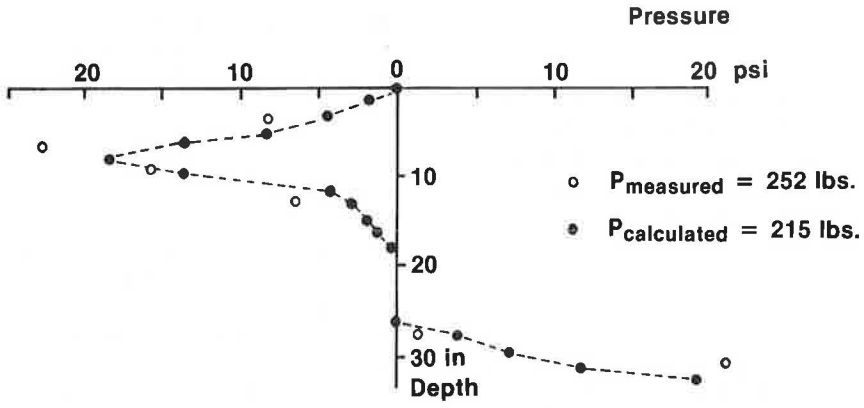

FIGURE 7 Lateral earth pressure comparison—sloping sand and upslope loading (Test no. Davis S-12).

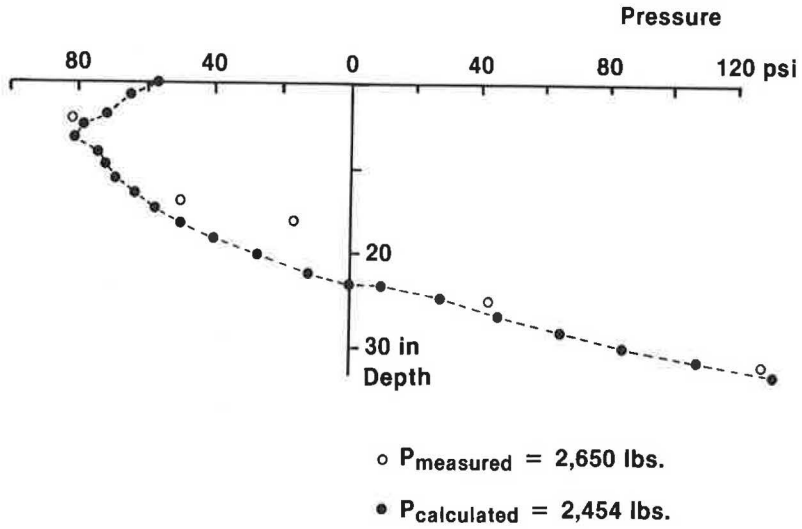

FIGURE 8 Lateral earth pressure comparison—level clay (Test no. Davis 7).

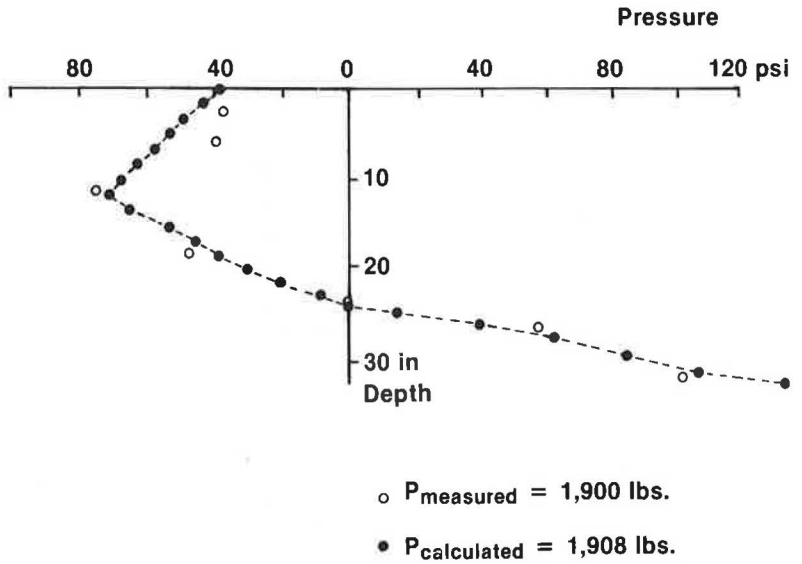

FIGURE 9 Lateral earth pressure comparison—sloping clay and downslope loading (Test no. Davis 10).

Level and Sloping Clayey Embankment

Two tests were studied and compared in this group: one on level ground (Test 7), the other on the sloping ground with the lateral load applied toward the slope (Test 10). The pressure distributions at lateral loads near or at failure were examined. Figures 8 and 9 indicate the individual comparisons. In general, fairly good agreement exists.

CONCLUSION

The research includes two major parts: a laboratory model study and an analytical formulation for detailed investigation of the laterally loaded CIDH piles. The model pile study was carried out in a test bin where both level and sloping embankments were constructed with either pit-run river sand or silty clay. An instrumented aluminum pipe pile was built to measure the load-versus-displacement relationship of the laterally loaded piles and the interface pressure distributions on the pile. The results were interpreted both quantitatively and qualitatively to describe the soil-structure interaction and the failure mechanism, and to compare with the analytical solutions.

The analytical solution was formulated on the basis of the failure wedge observed during the laboratory model pile tests and suggested by Reese et al. (*4*). Furthermore, Dubrova's movement-dependent lateral earth pressure distribution concept (*21*) was adopted and modified to calculate the interactive pressure distributions under all stages of lateral loading. A comprehensive set of design equations was developed applicable to both level and sloping ground.

Comparisons with model and field test results indicate that the proposed method of analysis is capable of predicting rea-

sonably well the magnitude and distribution of lateral earth pressure under various lateral loads for a wide range in pile geometry, soil conditions, and ground surface conditions. In particular, the nonlinear lateral earth pressure distributions at small lateral loads can be identified.

Though a relatively extensive comparison was made between the model test results (from this study and elsewhere) and the analytical predictions, additional field data are needed to further validate the usefulness of the developed formulation.

ACKNOWLEDGMENT

The authors are grateful for the financial and technical support provided by the California Department of Transportation.

REFERENCES

1. C. K. Shen, S. Bang, M. DeSalvatore, and C. J. Poran. Laterally Loaded Cast-In-Drilled-Hole Piles. In *Transportation Research Record 1191*, TRB, National Research Council, Washington, D.C., 1988, pp. 155–165.
2. B. B. Broms. Lateral Resistance of Piles in Cohesionless Soils. *Journal of the Soil Mechanics and Foundation Division*, ASCE, Vol. 90, No. SM2, 1964.
3. B. B. Broms. Lateral Resistance of Piles in Cohesive Soils. *Journal of the Soil Mechanics and Foundation Division*, ASCE, Vol. 90, No. SM3, 1964.
4. L. C. Reese, W. R. Cox, and F. D. Koop. Analysis of Laterally Loaded Piles in Sand. Presented at the Offshore Technology Conference, Paper No. 2080, Houston, Tex., May 1974.
5. H. Matlock. Correlations for Design of Laterally Loaded Piles in Soft Clay. Presented at the Offshore Technology Conference, Paper No. 1204, Houston, Tex., April 1970.
6. D. L. Ivey. *Theory, Resistance of a Drilled Shaft Footing to Overturning Loads*. Research Report 105-1. Texas Transportation Institute, Texas A&M University, College Station, Tex., Feb. 1968.
7. C. O. Hays, J. L. Davidson, E. M. Hagan, and R. R. Risitano. *Drilled Shaft Foundation for Highway Sign Structures*. Research Report D647F. Engineering and Industrial Experiment Station, University of Florida, Gainesville, Dec. 1974.
8. D. L. Ivey and W. A. Dunlap. *Design Procedure Compared to Full-Scale Tests of Drilled Shaft Footings*. Research Report 105-3. Texas Transportation Institute, Texas A&M University, Feb. 1970.
9. D. L. Ivey and L. Hawkins. Signboard Footings to Resist Wind Loads. *Civil Engineering*, Vol. 36, No. 12, Dec. 1966.
10. J. L. Davidson, C. O. Hays, and E. M. Hagan. Design of Drilled Shafts Supporting Highway Signs. In *Transportation Research Record 616*, TRB, National Research Council, Washington, D.C., 1976.
11. R. L. Lytton. *Design Charts for Minor Service Structure Foundations*. Research Report 506-1F. Texas Transportation Institute, Texas A&M University, Sept. 1971.
12. D. L. Ivey, K. J. Koch, and C. F. Raba. *Resistance of a Drilled Shaft Footing to Overturning Loads, Model Tests, and Correlation with Theory*. Research Report 105-2. Texas Transportation Institute, Texas A&M University, College Station, July 1968.
13. J. R. Seiler. Effect of Depth of Embedment on Pole Stability. *Wood Preserving News*. Vol. 10, No. 11, Nov. 1932.
14. J. B. Hansen. The Ultimate Resistance of Rigid Piles Against Transversal Forces. *Danish Geotechnical Institute Bulletin*, No. 12, Copenhagen, 1961.
15. V. R. Kasch, H. M. Coyle, R. E. Bartoskewitz, and W. G. Sarver. *Lateral Load Test of a Drilled Shaft in Clay*. Research Report 211-1. Texas Transportation Institute, Texas A&M University, College Station, 1977.
16. M. E. Bierschwale, H. M. Coyle, and R. E. Bartoskewitz. *Field Tests and New Design Procedure for Laterally Loaded Drilled Shafts in Clay*. Research Report 211-3F. Texas Transportation Institute, Texas A&M University, Jan. 1981.
17. G. L. Holloway, H. M. Coyle, R. E. Bartoskewitz, and W. G. Sarver. *Field Test and Preliminary Design Method for Lateral Loaded Drilled Shafts in Clay*. Research Report 211-2. Texas Transportation Institute, Texas A&M University, Sept. 1978.
18. N. F. Ismael and T. W. Klym. Behavior of Rigid Piers in Layered Cohesive Soil. *Journal of the Geotechnical Engineering Division*, ASCE, Vol. 104, No. GT8, Aug. 1978.
19. L. C. Reese. Design and Construction of Drilled Shafts. *Journal of the Geotechnical Engineering Division*, ASCE, Vol. 104, No. GT1, Jan. 1978.
20. W. V. Wright, H. M. Coyle, R. E. Bartoskewitz, and L. J. Milberger. *New Retaining Wall Design Criteria Based on Lateral Earth Pressure Measurements*. Research Report 169-4F. Texas Transportation Institute, Texas A&M University, Aug. 1975.
21. M. E. Harr. *Foundations of Theoretical Soil Mechanics*. McGraw-Hill, New York, 1966.
22. R. F. Scott. *Foundation Analysis*. Prentice-Hall, Englewood Cliffs, N.J., 1981.
23. C. K. Shen and S. Bang. *Lateral Resistance of Cast-In-Drilled-Hole Piles*. California Department of Transportation, Sacramento, 1989.
24. J. I. Adams and H. S. Radhakrishna. The Lateral Capacity of Deep Augered Footings. *Proc. of the 8th International Conference on Soil Mechanics and Foundation Engineering*, Vol. 2.1, Moscow, USSR, 1973.

Publication of this paper sponsored by Committee on Subsurface Soil-Structure Interaction.